OPTIMISING LANDSLIDE-TSUNAMI PREDICTION BASED ON PHYSICAL MODEL TESTS

Valentin Heller & Johannes Spinneken

Department of Civil and Environmental Engineering, Imperial College London, London SW7 2AZ, UK
E-mail: v.heller@imperial.ac.uk

Abstract

Subaerial landslide-tsunamis and impulse waves are generated by mass movements such as landslides, rock falls or glacier calving. To predict landslide-tsunamis (impulse waves) a number of empirical formulae have been proposed. Unfortunately, if they are applied to the 1958 Lituya Bay case, the prediction of the tsunami height or amplitude is varying by up to a factor of five. At first sight, the experimental conditions under which the various formulae were devised appear to be very similar. However, subtle differences in the experimental set-up may lead to considerable deviations in the empirical predictions.

To address this shortcoming, a comparative experimental study is presented. This study focuses on block model experiments being undertaken in a wave flume. The overall test programme concerns the investigation of three commonly ignored block model parameters: (i) the blockage ratio, (ii) the slide front angle and (iii) the transition at the slope toe. A systematical parameter variation is on-going. Herein, the experimental set-up, the repeatability and initial results based on the variation of (i) and (ii) are presented.

Results from repeated tests suggest that the methodology applied herein is highly repeatable, considering that landslide-tsunami prediction is associated with a considerable uncertainty. One test for each parameter configuration was therefore regarded as sufficient. Both test parameters (i) and (ii) above were found to significantly affect the wave features: the relative wave amplitudes vary up to 37% due to (i) and up to 76% due to (ii).

Those results help not only decreasing the discrepancies between landslide-tsunami predictions based on different empirical equations, but are also the first step in filling an important gap: to consider the effect of the slide type (block versus granular model slide) in generic predictive formulae. This will directly aid in predicting the effects of landslide-tsunamis (impulse waves) with higher reliability.

Introduction

Subaerial landslide-tsunamis (or impulse waves if they occur in a reservoir or lake) are generated by mass movements such as landslides, rock falls, shore instabilities or glacier calving. The most devastating examples include the 1963 Vaiont case in North-Italy, where such a wave overtopped a dam by more than 70 m and killed about 2000 people (Schnitter 1964), and the 1958 Lituya Bay case where a landslide-tsunami destroyed the forest up to a run-up height of 524 m above mean sea level (Miller 1960).

Landslide-tsunamis and impulse waves need to be predicted reliably on many occasions, including the planning and operation phases of reservoirs or when a slide starts to creep above a water body. Such predictions seek to reduce risk for both humans and infrastructure. To predict subaerial landslide-tsunamis, a number of empirical formulae have been proposed. Heller and Hager (2010) directly compare their work with 11 approaches from Kamphuis and Bowering (1972), Huber and Hager (1997), Monaghan and Kos (2000), Walder et al. (2003), Fritz et al. (2004), Panizzo et al. (2005), Zweifel et al. (2006), among others. The formulae are functions of the slide parameters, the hill slope angle and the water depth. Unfortunately, if they are applied to the Lituya Bay case, the prediction of the tsunami height or amplitude is varying by up to a factor of five (Heller and Hager 2010).

Apparent reasons for these discrepancies are that equations based on wave channel (2D) and wave basin experiments (3D) should not be compared (Heller et al. 2011, Watt et al. 2012). However, even if only 2D equations are compared, the variation is still up to a factor of three. Further explanations for these discrepancies are that some equations were applied outside their parameter limitations, the occurrence of significant scale effects in some studies and the use of different measurement systems. Moreover, studies are based on different slide types namely rigid (Kamphuis and Bowering 1972, Monaghan and Kos 2000, Walder et al. 2003, Panizzo et al. 2005, Heller et al. 2011, among others) and granular slides (Huber and Hager 1997, Fritz et al. 2004, Zweifel et al. 2006, Heller and Hager 2010, among others).

Nevertheless, predictions based on the same 2D slide model still vary considerably and Heller and Kinnear (2010) postulated that a large part of these discrepancies can be resolved if the effects of three commonly ignored block model parameters are investigated: (i) the blockage

ratio (slide width b_s relative to channel width b), (ii) the slide front angle and (iii) the transition at the slope toe.

Typical values for those three parameters (i)-(iii) were selected based on the block model studies reviewed in Heller and Kinnear (2010). The three investigated blockage ratios are b_s/b = 0.98, 0.96 and 0.88. More extreme values were excluded since wall effects may become too dominant for slides with b_s/b > 0.98 and 3D effects may be significant for b_s/b < 0.88. This study covers further the whole range of previously investigated slide front angles with 30, 45, 60 and 90°. All previous block model studies worked with none or a curved transition at the slope toe (Heller and Kinnear 2010). Those two extreme cases are also considered herein.

The long-term research goal is to improve the reliability of landslide-tsunami hazard assessment based on empirical equations. The variation of the parameters (i)-(iii) above is also a key aspect in understanding the effect of the slide type (block versus granular slide model), since those relevant block model parameters are of no (i) or of much less (ii, iii) relevance for granular slides: granular slides employ the whole channel width, the slide front angle is not an independent parameter and they can also better cope with an abrupt transition. This proceeding is a first step towards this long-term goal, aims to describe the methodology, evaluates the test repeatability, and presents initial results based on the variation of parameters (i) and (ii).

Methodology

The experiments were conducted in the Hydrodynamics Laboratory of the Department of Civil and Environmental Engineering at Imperial College London. The employed Coastal Wave Flume is 24.5 m long, b = 0.600 m wide and 1.0 m high; all its boundaries being made of glass. The ramp shown in Figure 1 was built with the front inclined at α = 45°, and was placed at the front end of the flume. The slope surface consisted of two PVC sheets, both covering the whole length, placed side-by-side. A stainless steel guide between the two sheets, matching a chamfer in the slide bottoms, assured that the slides stayed in the channel centre during impact. The slides were moved in the raised position with a pulley system (Figure 1) and released with a release mechanism fitted on the slide surface. Silicon sealant between the PVC sheets and the flume walls avoided any significant movements of the ramp. The glass bottom in the immediate slide impact zone was protected with a 1 m long and 2 mm thick rubber sheet covered with a 2 mm thick stainless steel plate. In addition, mastic sealer was placed at the bottom of the slope to assure that the slide comes to an immediate rest in the scenario without transition (Figure 1), such as in the study of Heinrich (1992).

The tsunami-waves were generated with rigid slides made of PVC. The slide parameters are defined in Figure 1 for a slide with a front angle ϕ = 45°. Those parameters are the slide volume $\forall_s$, slide density ρ_s, slide mass m_s, slide thickness s and total slide length l_s. The coordinate origin (x; z) is defined at the intersection of the still water surface and the hill slope ramp. This is also the origin of the x'-coordinate along the hill slope. The water depth is h. The most relevant wave parameters are the wave amplitude a, the wave height H and the wave period T, being defined as the time between two consecutive wave zero up-crossings.

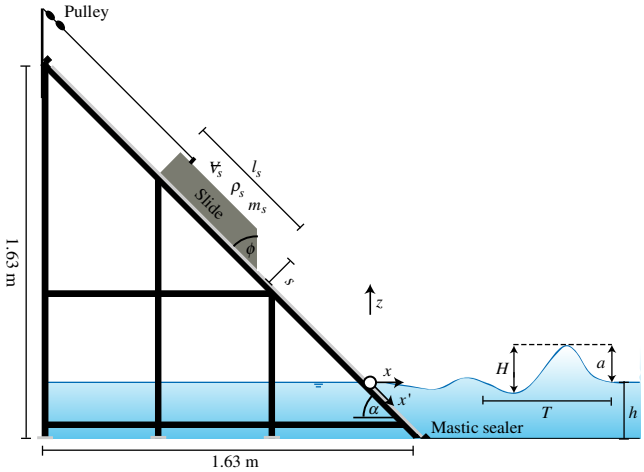

Figure 1: Ramp with pulley system, slide and wave parameters.

Table 1: Experimental parameters of 36 tests conducted to date; all slide thicknesses are s = 0.120 m ± 0.4%, slide volumes $\forall_s$ = 0.0373 m^3 ± 0.5%, slide densities ρ_s = 1537 kg/m^3 ± 0.5% and all configurations were tested without a transition.

Slide front angle ϕ (°)	Blockage ratio b_s/b (-)	Slide mass m_s (kg)	Total slide length l_s (m)	Water depth h (m)	Slide front release position x' (m)
90	0.980	57.40	0.526	0.300	0.00, –0.50, –1.10
				0.600	0.00, –0.30, –0.70
	0.963	57.47	0.539	0.300	0.00, –0.50, –1.10
				0.600	0.00, –0.30, –0.70
	0.877	57.29	0.587	0.300	0.00, –0.50, –1.10
				0.600	0.00, –0.30, –0.70
45	0.977	57.17	0.579	0.300	0.00, –0.50, –1.10
				0.600	0.00, –0.30, –0.70
	0.963	57.28	0.592	0.300	0.00, –0.50, –1.10
				0.600	0.00, –0.30, –0.70
	0.877	57.11	0.640	0.300	0.00, –0.50, –1.10
				0.600	0.00, –0.30, –0.70

The slide features are shown in Table 1. For all experiments, the slide thickness s ≈ 0.120 m, the slide volume $\forall_s$ ≈ 0.0373 m^3 and the slide density ρ_s ≈ 1537 kg/m^3 were held constant. The six slides were constructed with two slide bases which were modified with PVC additions screwed on the sides and/or rear resulting in three slide geometries for each base with constant volume

as shown in Figure 2. The test programme to date includes three blockage ratios b_s/b, two slide front angles ϕ and the configuration without a transition (Table 1). The two water depths (h = 0.300 m and 0.600 m) were in the range of insignificant scale effects (Heller et al. 2008, Heller 2011). For h = 0.600 m, the whole slide was submerged when the slide reached its final position, whereas with h = 0.300 m the rear part of the slide remained above the water surface. The slide front release positions were x' = 0.00, – 0.50 and –1.10 m (h = 0.300 m) and 0.00, – 0.30 and – 0.70 m (h = 0.600 m), resulting in centroid impact velocities $1.32 \leq V_s \leq 3.56$ m/s and different wave types (Heller and Hager 2011).

A set of dimensionless parameters is introduced based upon the definitions in Heller and Hager (2010). This includes the slide Froude number $0.58 \leq \mathsf{F} = V_s/(gh)^{1/2} \leq 2.07$ with g as the gravitational acceleration, the relative slide thickness $0.20 \leq S = s/h \leq 0.40$ and relative slide mass $0.27 \leq M = m_s/(\rho_w b_s h^2) \leq 1.21$ with ρ_w as the water density. The range for the impulse product parameter is $0.17 \leq \mathsf{P} = \mathsf{F} S^{1/2} M^{1/4} \{\cos[(6/7)\alpha]\}^{1/2} \leq 1.19$.

The slide impact velocity V_s was determined from Laser Distance Sensor (LDS) measurements sampled at 128 Hz. A PVC strip with holes at constant intervals (Figure 2) was bonded on the top surface of the slides and this strip was scanned with the LDS. The velocity V_s was then calculated with the spatial and temporal interval between two holes before and after the hole corresponding to the slide centroid impact. The wave features were recorded at 128 Hz using seven resistance type wave gauges located at relative distances x/h = 3.0, 5.0, 7.5, 10.0, 15.0, 25.0 and 40.0 (for h = 0.300 m) or 29.5 (for h = 0.600 m). Photographs of selected runs were taken with a digital camera.

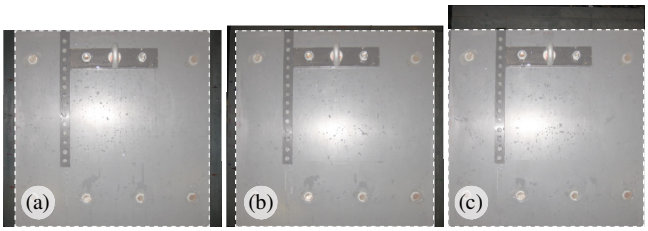

Figure 2: Plane view of slides consisting of a base (marked in white) and of additions screwed to the sides and/or rear to vary the blockage ratios from (a) 0.98, (b) 0.96 to (c) 0.88, but to hold the slide volume constant; fittings in the slide centre were used to connect the pulley system and a crane hook.

Results and Discussion

Overview

This section gives a general overview of the test procedure, addresses the relatively high repeatability of the experiments, and illustrates the relevance of the work based on the 36 tests conducted to date. Four tests are highlighted herein and they are named as I, II, III and IV. Figure 3 shows photographs of the wave generation and propagation of test I. The test parameters are: still water depth h = 0.300 m, slide front angle ϕ = 45°, blockage ratio b_s/b = 0.88, slide Froude number F = 1.33, relative slide thickness S = 0.40, relative slide mass M = 1.21 and impulse product parameter P = 0.78.

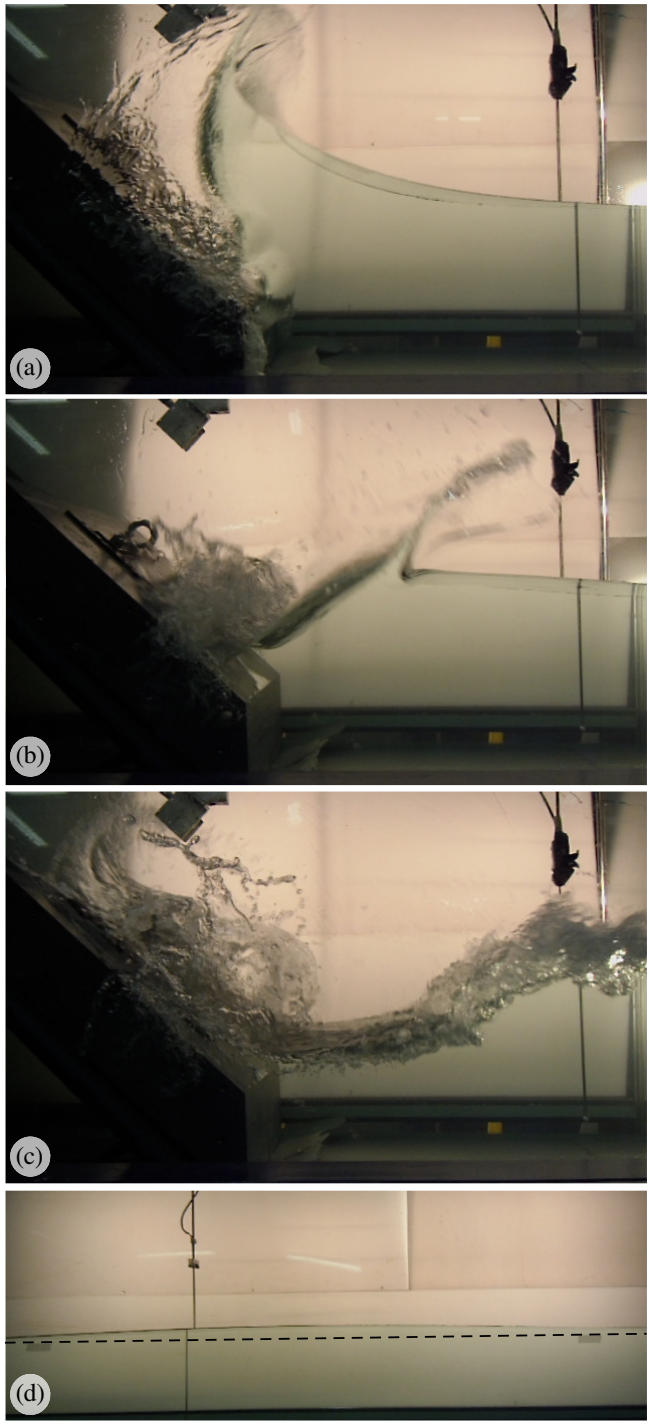

Figure 3: Slide impact and impulse wave generation of test I with h = 0.300 m, ϕ = 45°, b_s/b = 0.88, F = 1.33, S = 0.40, M = 1.21 and P = 0.78; wave generation (a) at t, (b) at t + 0.27 s and (c) at t + 0.40 s and wave propagation (d) at wave probe 7 (x/h = 40.0) with (--) initial still water surface.

The LDS and the first wave probe at x/h = 3.0 are shown on top of Figures 3(a), (b) and (c). In Figure 3(a), the slide generates an impact crater and part of the water on both sides of the slide is not or not fully displaced by the slide due to the 6% gaps (b_s/b = 0.88) between slide and channel walls. At the point of time shown, the slide front reaches the slope toe where it stops immediately due to the abrupt transition and the mastic sealer. The crater collapses in Figure 3(b) and generates the leading wave, which is also the largest wave in this test. The top of the crater results in a water splash reaching as far as the first wave probe in Figure 3(b). The collapsing impact crater also generates a bore-like wave running over the slide. This bore reaches the rear end of the slide in Figure 3(c), and the maximum of the leading wave simultaneously reaches wave probe 1.

Figure 3(d) shows a photograph of the leading wave of the same test in the wave propagation zone at wave probe 7 (x/h = 40.0). The flume section shown is approximately 2.5 m wide and the dashed line indicates the initial still water surface. The steep and large wave in Figure 3(c) has decreased considerably, and its length is several meters in Figure 3(d).

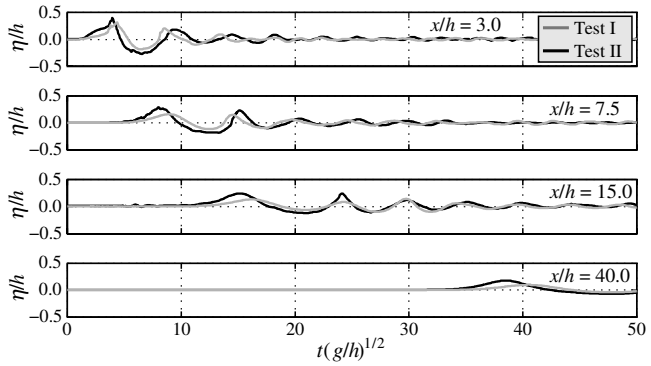

Figure 4: Effect of slide front angle ϕ and blockage ratio b_s/b on wave profiles of test I (ϕ = 45º, b_s/b = 0.88) and test II (ϕ = 90º, b_s/b = 0.98); the origin of the time scale is selected such that the wave fronts of the leading waves overlap.

To provide an indication of the magnitude of the discrepancies between two cases, Figure 4 shows relative water surface elevations η/h of tests I and II. The data are recorded with wave probes 1 (x/h = 3.0), 3 (x/h = 7.5), 5 (x/h = 15.0) and 7 (x/h = 40.0), and shown as a function of the relative time $t(g/h)^{1/2}$. The slide front angle ϕ and the blockage ratio b_s/b are different namely for test I ϕ = 45° and b_s/b = 0.88 and for test II ϕ = 90° and b_s/b = 0.98. The wave profiles vary significantly and none of the 11 approaches compared in Heller and Hager (2010) can consider these effects, since they all exclude ϕ and b_s/b. It is important to note that b_s/b is only indirectly included in $M = m_s/(\rho_w b_s h^2)$ in Heller and Hager (2010) via b_s, as discussed later on.

Repeatability

A critical aspect of physical modelling is the controllability of the governing parameters (slide impact velocity, slide thickness, slide volume etc.) in order to reach a high repeatability of the a priori unknown wave parameters (wave height, amplitude, period etc.). Most governing slide parameters are well controlled, as was already demonstrated in the caption of Table 1, where the deviations between different set-ups were in the order of less than one per cent.

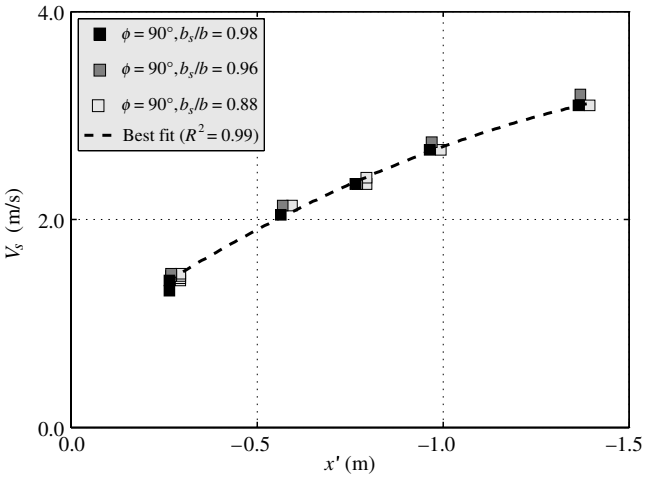

Figure 5: Slide centroid impact velocity V_s versus centroid release position x' along the ramp surface for ϕ = 90º.

An indication of the controllability of the most important parameter on landslide-tsunami generation, namely the slide impact velocity V_s (or slide Froude number F in dimensionless form), is demonstrated in Figure 5. It shows the calculated centroid slide impact velocity V_s as a function of the slide centroid release position x' (Figure 1) for all tests conducted with ϕ = 90°. Note that the slide centroid position in slide length direction changes with the blockage ratio (Figure 2), and the constant slide front release positions in Table 1 do therefore not correspond to constant travel distances of the slide centroid until its impact into the water body. This explains the systematic variation of V_s relative to the abscissa with the blockage ratio (colour) in Figure 5. Nevertheless, an excellent coefficient of determination R^2 = 0.99 for the best fit demonstrates that the measurement methodology of V_s with the LDS results in consistent values.

Table 2 shows the repeatability of the most relevant wave parameters based on test III (F ≈ 0.84) and IV (F ≈ 1.38). Both tests were conducted three times and Table 2 includes the wave amplitude a, wave height H and wave period T measured with wave probes 1 (x/h = 3.0), 3 (x/h = 7.5), 5 (x/h = 15.0) and 7 (x/h = 40.0). Deviations from the individual tests from the mean of all three tests are typically less than ±3%. The largest deviations are still within ±10%. Test IV with a larger slide Froude number F tends to result

in larger deviations than test III. This may be partially explained with the larger water splash and higher degree of turbulence observed in test IV.

Table 2: Repeatability of wave amplitude a, wave height H and wave period T for wave probe 1 (x/h = 3.0), 3 (x/h = 7.5), 5 (x/h = 15.0) and 7 (x/h = 40.0) with ± maximum deviations from the corresponding mean of three runs.

	Test III ($\mathsf{F} \approx 0.84$)				Test IV ($\mathsf{F} \approx 1.38$)			
Parameter	First run 1	Repetition 1	Repetition 2	Max. deviations from mean (%)	First run	Repetition 1	Repetition 2	Max. deviations from mean (%)
a_1 (mm)	63.1	63.3	62.9	+0.3 −0.3	103.3	104.7	100.5	+1.8 −2.3
a_3 (mm)	40.4	41.5	43.3	+3.8 −3.2	65.2	61.4	72.9	**+9.6 −7.7**
a_5 (mm)	33.4	34.2	35.9	**+4.1 −3.2**	52.4	50.2	54.4	+4.0 −4.1
a_7 (mm)	25.1	25.7	27.0	+4.1 −3.2	39.2	38.6	40.2	+2.2 −1.9
H_1 (mm)	88.2	88.1	90.1	+1.5 −0.8	176.4	184.2	179.9	+2.2 −2.1
H_3 (mm)	62.2	64.2	66.1	+3.0 **−3.1**	112.6	110.5	121.6	**+5.8 −3.8**
H_5 (mm)	49.2	50.6	52.3	**+3.2** −3.0	84.8	80.4	85.5	+2.3 −3.8
H_7 (mm)	36.6	37.5	38.5	+2.6 −2.5	56.4	55.5	56.8	+1.0 −1.3
T_1 (s)	1.22	1.23	1.22	+0.5 −0.3	1.36	1.37	1.37	+0.2 −0.5
T_3 (s)	1.81	1.82	1.85	+1.3 −0.9	1.77	1.79	1.77	+0.8 −0.4
T_5 (s)	2.55	2.47	2.29	**+4.7 −6.0**	2.3	2.24	2.21	+2.2 −1.8
T_7 (s)	3.25	3.25	3.33	+1.6 −0.8	3.52	3.41	3.33	**+2.9 −2.6**

Normally, measurement data used to devise empirical equations for subaerial landslide-tsunamis scatter at least by ±30% relative to a and H and much more relative to T (Heller and Hager 2010). In some studies, the scatter is in the order of +100/–50% relative to a/h or H/h (e.g. Walder et al. 2003, Panizzo et al. 2005), and the results for the wave period are often not even presented. The maximum deviations of +9.6/–7.7% found in Table 2 can therefore be considered as relatively small, and this supports the decision to conduct each test only once in this study.

Initial results

The relative wave amplitudes a/h at x/h = 7.5 of all 36 tests conducted to date are compared in Figure 6 as a function of the impulse product parameter P. The relative amplitudes of the tests involving a slide front angle $\phi = 90°$ are up to 76% larger than for tests with $\phi = 45°$, if comparing experiments with identical blockage ratios. The effect of ϕ on the relative wave amplitude tends to increase with increasing P (corresponding to an increasing F). Also the blockage ratio b_s/b has a systematic effect on a/h. Slides with b_s/b = 0.98 (black symbols) generate consistently larger waves than slides with b_s/b = 0.88 (light grey symbols), irrespective of the slide front angle. The variation of a/h with b_s/b is up to 37% depending on the value of P.

Figure 7 shows the relative wave heights H/h at x/h = 7.5 as a function of the impulse product parameter P. The conclusions derived from Figure 7 are similar to the ones already found above for the relative wave amplitude: both the slide front angle and the blockage ratio have a significant effect on the wave features. The wave height is defined as the sum of the wave amplitude (shown in Figure 6) and the wave trough. Since the results in Figures 6 and 7 are very similar, it can be concluded that the slide front angle and the blockage ratio seem to affect both the wave amplitude and the wave trough similarly.

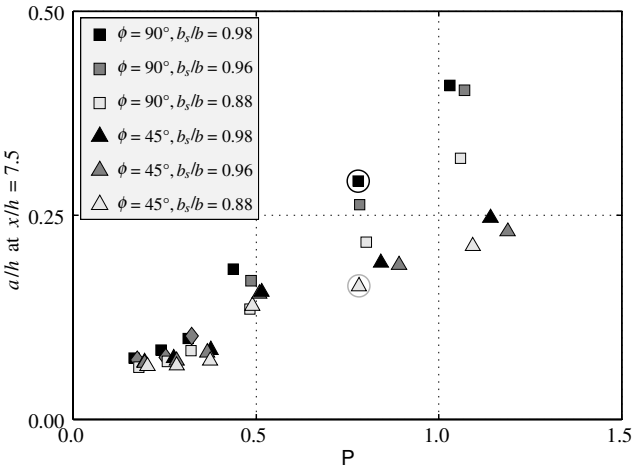

Figure 6: Relative wave amplitude a/h at x/h = 7.5 versus impulse product parameter $\mathsf{P} = \mathsf{F}S^{1/2}M^{1/4}\{\cos[(6/7)\alpha]\}^{1/2}$ for the 36 experiments shown in Table 1; the two values resulting from the wave profiles shown in Figure 4 are encircled.

Figures 6 and 7 show that the relative wave amplitudes and heights increase with increasing blockage ratio. The slide width is not only included in the blockage ratio, but also in the impulse product parameter P through $M = m_s/(\rho_w b_s h^2)$. The relative wave amplitude or height increases with increasing P (Heller and Hager 2010). Since b_s is considered in the denominator of M, a decreasing b_s results in a larger P and larger waves, respectively. This is in marked contrast to the results shown in Figure 6. It is also important to note that the parameter M was not developed to consider the blockage ratio but rather to consider the slide mass and density. In fact, the consequences of the blockage ratio have not been investigated to date, and it is irrelevant for granular slides filling the whole channel width. Developing a methodology that incorporates the blockage ratio in empirical formulae is an important point which needs to be addressed in the near future.

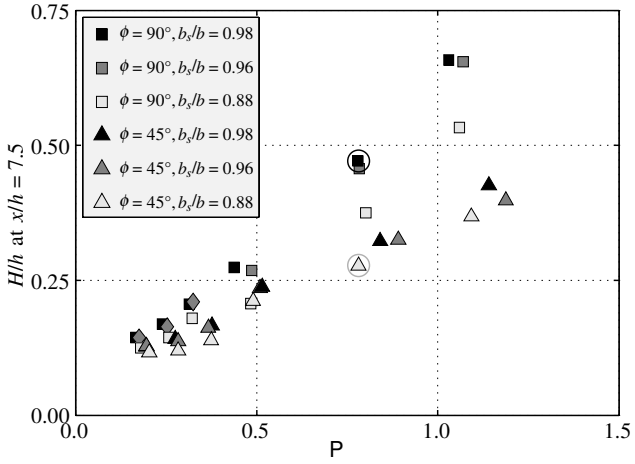

Figure 7: Relative wave height H/h at x/h = 7.5 versus impulse product parameter $P = FS^{1/2}M^{1/4}\{\cos[(6/7)\alpha]\}^{1/2}$ for the 36 experiments shown in Table 1; the two values resulting from the wave profiles shown in Figure 4 are encircled.

Conclusions and Outlook

This paper presents the methodology, the test repeatability and initial results of a physical landslide-tsunami (impulse wave) study. The purpose of the present work is to fully understand differences between landslide-tsunamis generated by block and granular slide models, and also to improve the reliability of tsunami prediction. The 36 test conducted to date include the variation of two block model parameters, namely the slide front angle (ϕ = 45 and 90º) and the blockage ratio (slide width/channel width = 0.98, 0.96 and 0.88).

The governing parameters including the slide features and the slide impact velocity are shown to be well controlled in this study. The maximum variation between the wave features from the mean for tests and its two repetitions was +9.6/–7.7%. This can be considered as a good repeatability given that the wave amplitude or height prediction of subaerial landslide-tsunamis (impulse waves) are in some studies associated with a data scatter in the order of +100/ –50%. The main tests were therefore only conducted once.

Initial results of 36 tests clearly show the relevance of the investigated parameters in the present study: the slide front angle changes the relative wave amplitude by up to 76% and the blockage ratio by up to 37% at a characteristic location. Similar conclusions follow from the analysis of the relative wave height at the same location. This indicates that landslide-tsunami (impulse wave) prediction may suffer from significant uncertainties since those two parameters are excluded in predictive empirical equations.

Future work will conclude this systematic parameter variation. This will include two additional slide front angles (ϕ = 30 and 60º) and also a circular-shaped transition at the slope toe. It is expected that the transition also has a significant effect on landslide-tsunami features and it is very likely that this effect is even larger than the effects of the slide front angle and the blockage ratio. The block model results will then be compared with the granular slide data of Heller and Hager (2010) with the aim to fully quantify the effect of the slide type on landslide-tsunamis; the overall aim being to improve the reliability in landslide-tsunamis (impulse waves) predictions.

Acknowledgement

The position of VH is funded by an Imperial College London Junior Research Fellowship.

References

Fritz, H.M., Hager, W.H., & Minor, H.-E. (2004). Near field characteristics of landslide generated impulse waves. *Journal of Waterway, Port, Coastal, and Ocean Engineering* 130(6), 287-302.

Heinrich, P. (1992). Nonlinear water waves generated by submarine and aerial landslides. *Journal of Waterway, Port, Coastal, and Ocean Engineering* 118(3), 249-266.

Heller, V. (2011). Scale effects in physical hydraulic engineering models. *Journal of Hydraulic Research* 49(3), 293-306.

Heller, V., & Hager, W.H. (2011). Wave types in landslide generated impulse waves. *Ocean Engineering* 38(4), 630-640.

Heller, V., Moalemi, M., Kinnear, R.D., & Adams, R.A. (2011). Geometrical effects on landslide generated tsunamis. *Journal of Waterway, Port, Coastal, and Ocean Engineering* (preview manuscript).

Heller, V., & Hager, W.H. (2010). Impulse product parameter in landslide generated impulse waves. *Journal of Waterway, Port, Coastal, and Ocean Engineering* 136(3), 145-155.

Heller, V., & Kinnear, R.D. (2010). Discussion of "Experimental investigation of impact generated tsunami; related to a potential rock slide, Western Norway" by G. Sælevik, A. Jensen, G. Pedersen [Coastal Eng ineering 56(2006), 897-906]. *Coastal Engineering* 57(8), 773-777.

Heller, V., Hager, W.H., & Minor, H.-E. (2008). Scale effects in subaerial landslide generated impulse waves. *Experiments in Fluids* 44, 691-703.

Huber, A., & Hager, W.H. (1997). Forecasting impulse waves in reservoirs. *Proceeding of the 19th Congrès des Grands Barrages, Florence*, ICOLD, Paris, 993-1005.

Kamphuis, J.W., & Bowering, R.J. (1972). Impulse waves generated by landslides. 12th *International Conference on Coastal Engineering*. Washington DC, USA, 1. ASCE, New York, pp. 575-588.

Miller, D.J. (1960). Giant waves in Lituya Bay, Alaska. *Geological Survey Professional Paper No.* 354-C, U.S. Government Printing Office, Washington, D.C.

Monaghan, J.J., & Kos, A. (2000). Scott Russell's wave generator. *Physics of Fluids* 12(3), 622-630.

Panizzo, A., De Girolamo, P., & Petaccia, A. (2005). Forecasting impulse waves generated by subaerial landslides. *Journal of Geophysical Research* 110(C12025), 1-23.

Schnitter, G. (1964). Die Katastrophe von Vaiont in Oberitalien. *Wasser- und Energiewirtschaft* 56, 61-69 (in German).

Walder, J.S., Watts, P., Sorensen, O.E., & Janssen, K. (2003). Tsunamis generated by subaerial mass flows. *Journal of Geophysical Research* 108(B5), 2236(2) 1-19.

Watt, S.F.L., Talling, P.J., Vardy, M.E., Heller, V., Hühnerbach, V., Urlaub, M., Sarkar, S., Masson, D.G., Henstock, T.J., Minshull, T.A., Paulatto, M., Le Friant, A., Lebas, E., Berndt, C., Crutchley, G.J., Karstens, J., Stinton, A.J., & Maeno, F. (2012). Combinations of valcanic-flank and seafloor-sediment failure offshore Montserrat, and their implications for tsunami generation. *Earth and Planetary Science Letters* 319-320, 228-240.

Zweifel, A., Hager, W. H., & Minor, H.-E. (2006). Plane impulse waves in reservoirs. *Journal of Waterway, Port, Coastal, and Ocean Engineering* 132(5), 358-368.